

## Excitation function for the pion single-charge-exchange reaction $^{13}\text{C}(\pi^+, \pi^0)^{13}\text{N}(\text{g.s.})$

L. E. Ussery,\* D. J. Vieira, J. J. H. Berlijn,† G. W. Butler, B. J. Dropesky,  
G. C. Giesler, N. Imanishi,‡ M. J. Leitch,§ and R. S. Rundberg

*Isotope and Nuclear Chemistry Division, Los Alamos National Laboratory, Los Alamos, New Mexico 87545*

(Received 28 March 1988)

Angle-integrated cross-section measurements for the reaction  $^{13}\text{C}(\pi^+, \pi^0)^{13}\text{N}(\text{g.s.})$ , made with activation techniques, are presented for the energy range 50–350 MeV. These results are compared to earlier data for the same reaction and to differential cross-section measurements on other light nuclei. A deep minimum is observed near 70 MeV in the excitation function; it reflects the *s*- and *p*-wave interference minimum seen in the free-nucleon single-charge-exchange cross section. The data are compared to several optical-model calculations.

### I. INTRODUCTION

The study of pion single-charge-exchange (SCX) reactions is currently of strong interest in intermediate-energy nuclear science because it provides a unique tool for advancing our understanding of pion-nucleus interactions. For example, because the pion-nucleus single-charge-exchange reaction proceeds exclusively via the isovector transition it provides a selective method for studying the isovector interaction. Since the advent of the meson factories, there have been many measurements of pion SCX.<sup>1,2</sup> These measurements are generally of two types, angle-integrated cross-section measurements made by means of activation techniques and differential cross-section measurements (primarily at forward angles) in which the outgoing  $\pi^0$  is detected. Most of these experiments involve isobaric analog state (IAS) transitions for which the nuclear structures of the initial and final states are nearly identical. One of the more interesting IAS single-charge-exchange reactions is  $^{13}\text{C}(\pi^+, \pi^0)^{13}\text{N}(\text{g.s.})$  for which the ground state is the only particle-bound state of  $^{13}\text{N}$  and decays by positron emission with a half-life of 9.96 min. Thus this reaction is well suited to measurement by activation techniques.

The earliest measurements of this reaction cross section were by Chivers *et al.*,<sup>3</sup> who reported a cross section of 3.0 mb in the pion-nucleon (3,3) resonance region at 180 MeV. In a later measurement covering the energy range of 70–250 MeV, Shamai *et al.*<sup>4</sup> observed a relatively flat excitation function with a cross section of 0.95 mb at 180 MeV. A number of theoretical calculations of the excitation function for this reaction have been performed recently using a variety of models.<sup>5–7</sup> However, all of these approaches predict a smaller cross section than observed, typically ranging from 0.2 to 0.5 mb at 180 MeV. Because of this unexplained discrepancy between theory and experiment and the suggestion<sup>8</sup> that the cross sections of Shamai *et al.* could be too large because of substantial contributions from the secondary reaction  $^{13}\text{C}(p, n)^{13}\text{N}$ , we decided to reinvestigate this SCX reaction. Presented here are new measurements of the  $^{13}\text{C}(\pi^+, \pi^0)^{13}\text{N}(\text{IAS})$  cross section over the energy range 50–350 MeV.

### II. EXPERIMENTAL

#### A. Pion channels

The measurements were performed at the Clinton P. Anderson Meson Physics Facility (LAMPF) on both the low-energy pion (LEP) channel<sup>9</sup> and the high-energy pion ( $P^3$ ) channel.<sup>10</sup> The LEP channel was used to obtain pions with incident energies from 50 to 190 MeV and fluxes of  $1 \times 10^7$  to  $4 \times 10^8$   $\pi^+$ /sec, respectively, and a momentum spread of 1–4%. The  $P^3$  channel was used for 120- to 350-MeV pions at fluxes of  $1.2 \times 10^8$  to  $1.8 \times 10^9$   $\pi^+$ /sec, respectively, and a momentum spread of 5–7%. Typical pion beam spot sizes for both channels were 1–3 cm vertical by 2–4 cm horizontal. Protons were removed from the pion beams by means of a differential energy-loss technique employing a degrader in the center of the channels. For pion energies of 300 MeV and below, the remaining proton flux is negligible. At 350 MeV, the proton contamination was estimated to be  $2 \pm 2\%$  of the pion flux based on previous measurements.<sup>11</sup> As the beam energy is lowered at LEP, positron contamination approaches  $e^+/\pi^+ \sim 0.4$  for 50-MeV pions,<sup>12</sup> however, because the  $e^+$  cross sections are much smaller than those for pions<sup>13</sup> these positrons give a negligible contribution to the  $^{13}\text{N}$  activity. Furthermore, their effect on the  $^{11}\text{C}$  monitor activity used to determine the pion flux is very small.<sup>11</sup>

#### B. Target irradiations and counting

The  $^{13}\text{C}$  targets were fabricated from 99.3% isotopically enriched  $^{13}\text{C}$  powder pressed into thin circular disks with 10% of a 90%-enriched  $^{13}\text{C}$  polyethylene binder. The resulting targets had a  $^{13}\text{C}$  enrichment of 98.4%, a diameter of 4.92 cm, and areal thicknesses ranging from 48 to 195 mg/cm.<sup>2</sup>

During a pion irradiation, each  $^{13}\text{C}$  target (or stack of targets) was contained in a thin polyethylene envelope to prevent recoiling  $^{13}\text{N}$  produced in the surrounding air via the  $^{14}\text{N}(\pi^+, \pi N)^{13}\text{N}$  and  $^{16}\text{O}(\pi^+, X)^{13}\text{N}$  reactions from contaminating the targets. Although the duration of the pion irradiations ranged from 5 to 30 min, they were usu-

ally about 15 min in order to optimize the yield of  $^{13}\text{N}$  relative to other species. A plastic scintillation detector was mounted near the target, but out of the beam, to observe scattered pions. This detector monitored beam intensity variations during each irradiation. If beam-off periods occurred, an appropriate correction was applied to the calculated cross section.

The pion intensity was determined by simultaneously irradiating a Pilot B plastic scintillator<sup>14</sup> disk (of the same diameter as the target and about 100 mg/cm<sup>2</sup> thick) that was located just downstream of the  $^{13}\text{C}$  target but outside of the polyethylene envelope. The plastic scintillator was activated by the  $^{12}\text{C}(\pi^+, \pi N)^{11}\text{C}$  reaction, for which the cross sections have been established over the energy range of interest.<sup>11,15</sup> After each irradiation, the scintillator disk was counted with a  $\beta^+$ - $\gamma$  coincidence system with which the absolute 20.38-min  $^{11}\text{C}$  activity was determined.<sup>16</sup>

After each irradiation, the  $^{13}\text{C}$  target was removed from the polyethylene envelope and the induced  $\beta^+$  activity was measured with an annihilation radiation  $\gamma$ - $\gamma$  coincidence counter. This counter consisted of two face-to-face 7.6-cm by 7.6-cm NaI(Tl) detectors with a 0.16-cm-thick copper plate placed in front of each detector with the  $^{13}\text{C}$  target between them to ensure that all the positrons were stopped and annihilated close to the target. This arrangement afforded maximum counter efficiency and prevented the summing of the two annihilation quanta in a single detector. To further increase the sensitivity of the system, the background of the counter was reduced by completely surrounding it with 10 cm of lead. The absolute efficiency of this system was determined by counting activated Pilot B disks on this counter and on the  $\beta$ - $\gamma$  coincidence system mentioned earlier. Counting of the activated targets started 2–15 min after the end of bombardment and continued for 60–120 min.

### C. Target impurity determinations

Contamination of the  $^{13}\text{C}$  targets, particularly by  $^{16}\text{O}$  and  $^{14}\text{N}$ , could contribute to the observed  $^{13}\text{N}$  yield and to other components in the decay curve. Therefore it was necessary to determine the amount of such target contaminations and the associated cross sections for  $^{13}\text{N}$  production in order to apply corrections to the SCX data. To determine the presence of such chemical contaminants in our  $^{13}\text{C}$  targets in a nondestructive manner, several sets of  $\pi^-$  irradiations were performed at an incident pion energy of 190 MeV. When the counting of the target was started on a local  $\beta^+$  counting system within 2–3 min after the end of a bombardment, a small component of 2.04-min  $^{15}\text{O}$  was observed and, in some cases, a very small  $^{13}\text{N}$  component was also observed. These observations confirmed the presence of  $Z > 6$  contaminants. Destructive chemical analyses of portions of two targets revealed 0.9% oxygen contamination by weight. Further chemical analyses indicated no significant contamination ( $< 0.1\%$  by weight) of nitrogen or other elements. Chemical analyses were also performed at widely separated times to determine if the level of contamination was varying with time; the oxygen con-

tamination was found to be essentially constant. However, as a precaution against the adsorption of water from the air, the targets were stored in a desiccator and handled with tweezers and gloves.

Because of the presence of oxygen in our  $^{13}\text{C}$  targets, small corrections were applied to our  $^{13}\text{N}$  decay data for the contributions of  $^{15}\text{O}$ ,  $^{13}\text{N}$ , and  $^{11}\text{C}$  radioactivities that resulted from  $\pi^+$  reactions with oxygen. To facilitate making this correction, we first measured the cross section for the  $^{16}\text{O}(\pi^-, \pi N)^{15}\text{O}$  reaction at 190 MeV by performing several  $\pi^-$  irradiations of  $\sim 215$  mg/cm<sup>2</sup> boric acid ( $\text{H}_3\text{BO}_3$ ) targets and determining the yield of  $^{15}\text{O}$ . From the measured  $^{15}\text{O}$  activity in the boric acid targets, we determined a cross section of  $62.2 \pm 1.9$  mb for the  $^{16}\text{O}(\pi^-, \pi N)^{15}\text{O}$  reaction, in agreement with a previous measurement.<sup>17</sup> Each  $^{13}\text{C}$  target was then irradiated with the 190-MeV  $\pi^-$  beam, and the  $^{15}\text{O}$  disintegration rate was determined. We proceeded to calculate the amount of oxygen present in each  $^{13}\text{C}$  target. Oxygen contaminations of target combinations were obtained by summing the contaminations of the individual targets in each stack. The oxygen contamination in our targets ranged from 0.4 to 1.1 % by weight, consistent with the destructive chemical analyses.

To check the reported cross sections<sup>15</sup> for  $\pi^+$  reactions on oxygen and to extend the measurements to cover the pion energies of interest for this study, a series of irradiations of the boric acid targets was performed with  $\pi^+$  energies from 50 to 350 MeV. As a result of these irradiations, cross sections for the following reactions were obtained:  $^{16}\text{O}(\pi^+, \pi N)^{15}\text{O}$ ;  $^{16}\text{O}(\pi^+, X)^{13}\text{N}$ ; and  $^{16}\text{O}(\pi^+, Y)^{11}\text{C}$ , where  $X$  and  $Y$  represent any combination of emitted particles that yields the final product. These cross sections are presented in Fig. 1 and are in good

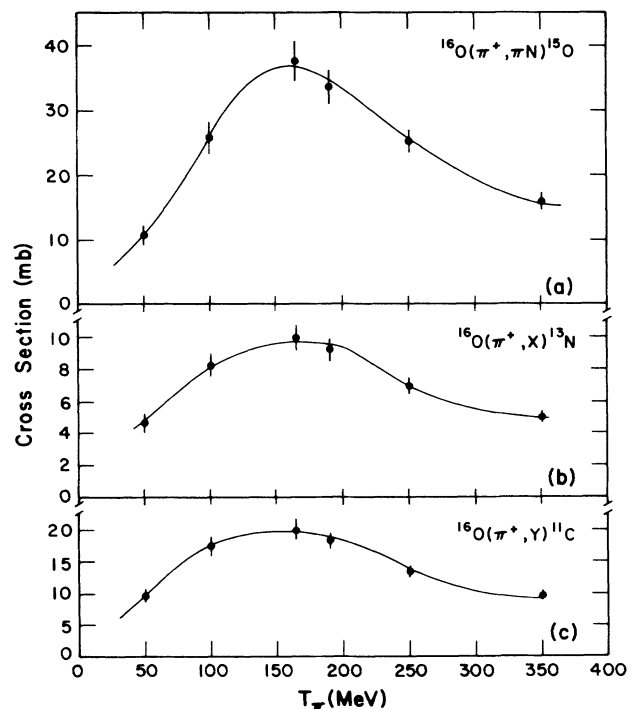


FIG. 1. Excitation functions for relevant  $\pi^+$  reactions in  $^{16}\text{O}$ . The smooth curves are to guide the eye.

agreement with those previously measured at much lower pion beam intensities.<sup>17</sup> Cross sections for pion energies falling between measured data points were obtained by interpolation. Using these cross sections and the measured oxygen contamination in each target, we corrected for the contributions of <sup>15</sup>O, <sup>13</sup>N, and <sup>11</sup>C resulting from  $\pi^+$  reactions with the oxygen present in each target.

#### D. Cross-section determination

Processing of the decay data obtained for each  $\pi^+$  irradiation consisted of a series of steps. Initially, each data set was analyzed with the decay code CLSQ.<sup>18</sup> The data from each Pilot B target were fitted to obtain the activity of <sup>11</sup>C produced by the pion irradiation. This yield was used in conjunction with the established cross section for the <sup>12</sup>C( $\pi^+$ , $\pi$ N)<sup>11</sup>C reaction<sup>11,15</sup> to determine the pion flux for each irradiation.

Most sets of decay data from the <sup>13</sup>C target irradiations exhibited two components, the 9.96-min half-life of <sup>13</sup>N and the 20.38-min half-life of <sup>11</sup>C. The latter activity arises from reactions such as <sup>13</sup>C( $\pi^+$ , $pn$ )<sup>11</sup>C, <sup>13</sup>C( $\pi^+$ , $\pi^+2n$ )<sup>11</sup>C, and <sup>12</sup>C( $\pi^+$ , $\pi$ N)<sup>11</sup>C on the 1.6% <sup>12</sup>C present in the <sup>13</sup>C targets. Generally, it was not feasible to fit the data for shorter half-life components ( $\leq 2$  min) because of the  $\sim 5$ -min time interval between the end of irradiation and the beginning of counting. Because oxygen was known to be present in the <sup>13</sup>C targets, analysis of the data from the <sup>13</sup>C target irradiations began with the determination of the contributions of <sup>11</sup>C, <sup>13</sup>N, and <sup>15</sup>O resulting from this contaminant. This was done by means of the measured beam flux for the particular irradiation, the measured oxygen contamination for the target, and the cross sections determined for the reactions <sup>16</sup>O( $\pi^+$ , $\pi$ N)<sup>15</sup>O, <sup>16</sup>O( $\pi^+$ , $X$ )<sup>13</sup>N, and <sup>16</sup>O( $\pi^+$ , $Y$ )<sup>11</sup>C. The <sup>15</sup>O activity obtained in this manner was then inserted into the decay curve analysis as a known component, and the data were fitted for total <sup>13</sup>N and <sup>11</sup>C activities. The <sup>13</sup>N yield determined from this analysis was corrected for the amount of <sup>13</sup>N from the <sup>16</sup>O( $\pi^+$ , $X$ )<sup>13</sup>N reaction. This correction reduced the <sup>13</sup>N yield by 2–17% depending on the particular target and irradiation energy. The corrected <sup>13</sup>N yield was then used to calculate a cross section for the single-charge-exchange reaction <sup>13</sup>C( $\pi^+$ , $\pi^0$ )<sup>13</sup>N for each irradiation.

#### E. Secondary ( $p, n$ ) corrections

A contribution to the total observed yield of <sup>13</sup>N also results from the secondary reaction <sup>13</sup>C( $p, n$ )<sup>13</sup>N. The protons that induce this latter reaction come from several sources: (1) those produced within the target as a result of pion-nucleus interactions; (2) those emitted in the backward hemisphere from pion interactions in the downstream Pilot B monitor disk; and (3) those that are contaminants in the pion beam.

The proton contamination of the beam is insignificant ( $< 0.1\%$ ) at all our pion energies except 350 MeV (corresponding to 111-MeV protons). A small correction was made for the contribution to the observed <sup>13</sup>N yield from these protons. These protons also contribute to the <sup>11</sup>C yield in the Pilot B monitor used to determine the pion

flux. This contribution results from the <sup>12</sup>C( $p, pn$ )<sup>11</sup>C reaction for which the cross sections are as large or larger than those for the <sup>12</sup>C( $\pi^+$ , $\pi$ N)<sup>11</sup>C reaction. A small correction was also made for this contribution.

Because the secondary protons from sources (1) and (2) above are low in energy and the cross sections for the ( $p, n$ ) reaction are large for these energies, especially compared to the ( $\pi^+$ , $\pi^0$ ) SCX cross sections, correction of the observed SCX cross sections for secondary contributions is essential. In order to determine the contributions to the <sup>13</sup>N yield from secondary ( $p, n$ ) reactions, we have developed an analytical formalism. This method, which is described in some detail in the Appendix and in complete detail elsewhere,<sup>19</sup> is briefly outlined as follows.

The energy spectrum and intensity of the secondary protons produced in the <sup>13</sup>C target as a result of pion-nucleus interactions are determined<sup>20</sup> by means of the ISOBAR (Ref. 21) intranuclear cascade code and the DFF (Ref. 22) evaporation code. A comparison of these calculated values with the experimental inclusive proton yield data of Carroll *et al.*<sup>23</sup> showed agreement within  $\sim 40\%$ . The uncertainty in our calculated proton spectrum and intensity represents the largest uncertainty in the secondary ( $p, n$ ) correction.

The angular distribution of the secondary protons was taken to be isotropic because a cosine dependence on the polar angle was found to cancel out upon integration of the reaction probability over angle and target thickness. The measured excitation function for the <sup>13</sup>C( $p, n$ )<sup>13</sup>N(g.s.) reaction was obtained from several sources.<sup>24–26</sup> Detailed information is only available for the cross sections from threshold energy (3.24 MeV) up to about 23 MeV; we assumed a  $1/E$  dependence<sup>27</sup> for the cross section above 23 MeV and used a measurement of the cross section at 155 MeV to determine the slope.<sup>26</sup> The tables of Williamson *et al.*<sup>28</sup> were used to relate the initial proton energy to the proton range in the target material. We also assumed that the protons traveled along straight lines in traversing the target.

The probability that a proton would undergo a ( $p, n$ ) reaction within a distance  $l$  in the target material as a function of the initial proton energy was computed. This probability formed the basis for calculating the average probability for a ( $p, n$ ) reaction to occur anywhere in the target. The pion energy was taken to be constant throughout the target thickness (a 164-MeV pion loses only 1.2 MeV in traversing 660 mg/cm<sup>2</sup> of <sup>13</sup>C). Thus a straightforward integration of the ( $p, n$ ) reaction probability averaged over the target thickness and over all angles was carried out.

To determine the effect of the pion beam size on secondary ( $p, n$ ) contributions, a calculation was carried out for two beam radii, 0.75 and 1.50 cm, for a target radius of 2.46 cm. The overall secondary reaction contribution for the larger beam radius was found to be less than 1% smaller than that for the smaller radius.

Finally, the secondary ( $p, n$ ) contribution to the <sup>13</sup>N yield that arises from secondary protons originating in the downstream Pilot B monitor disk (average thickness 105.8 mg/cm<sup>2</sup>) and induces ( $p, n$ ) reactions in the <sup>13</sup>C target was taken into account. This calculation used the

basic approach described above, with only minor modification. Because protons from the cascade are predominantly forward peaked, only evaporation protons were assumed to contribute to this part of the secondary reactions. The secondary contribution from these protons originating in the monitor disk was approximately 10% of the contribution from protons originating in the  $^{13}\text{C}$  target itself.

In Fig. 2 we show the calculated contribution to the observed SCX cross section that is due to the secondary ( $p,n$ ) reaction as a function of incident pion energy and target thickness. This contribution, as one might expect, rises to a broad peak in the vicinity of the (3,3) resonance where secondary proton production should be at a maximum. The dramatic increase in secondary ( $p,n$ ) reactions with target thickness is consistent with the peaking of the ( $p,n$ ) cross section at low energies. Figure 3, on the other hand, shows the secondary reaction contribution at 162-MeV pion kinetic energy plotted as a function of target thickness with its band of uncertainty (lower portion of figure) and the average correction curve drawn through our weighted average data points (upper portion). These data, including corrections for oxygen contamination, were compiled from measurements made with single targets or combinations of stacked targets. Within the uncertainties of the experimental data and of the secondary corrections, there is good agreement. For comparison, a measurement by Shamai *et al.*<sup>4</sup> at 162 MeV is also plotted. This data point has its secondary ( $p,n$ ) correction removed and does not include a correction for oxygen contamination. It was assumed by Shamai *et al.* that no oxygen correction was required. Extrapolation of our data to the target thickness of their measurement is inconsistent with their cross-section determination. A possible explanation for this discrepancy is discussed later.

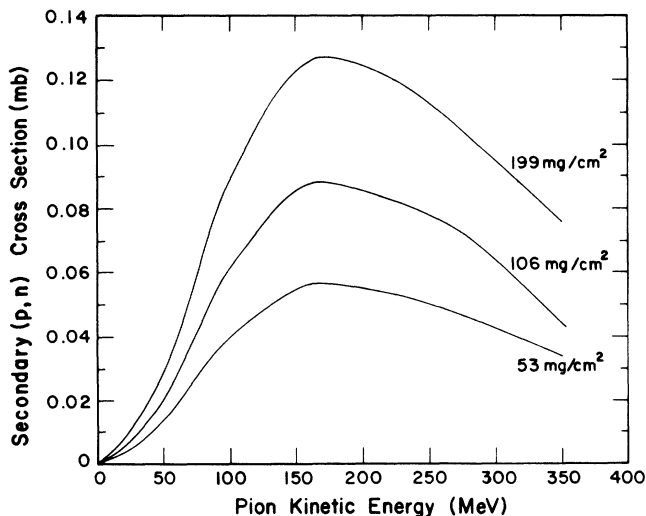


FIG. 2. Calculated cross sections for the secondary reaction  $^{13}\text{C}(p,n)^{13}\text{N}$  as a function of pion kinetic energy and target thickness.

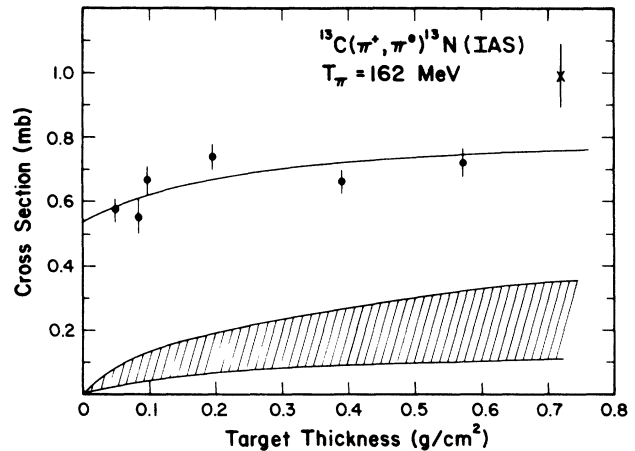


FIG. 3. Cross sections measured in this study ( $\bullet$ ) for the  $^{13}\text{C}(\pi^+, \pi^0)^{13}\text{N}$  reaction at 162 MeV as a function of target thickness (data corrected for oxygen contamination). The shaded band represents the range of calculated  $^{13}\text{C}(p,n)^{13}\text{N}$  cross sections due to secondary protons. The solid curve through the experimental points corresponds to the mean of the calculated ( $p,n$ ) contribution added to the basic ( $\pi^+, \pi^0$ ) cross section of 0.54 mb. Measurement of Shamai *et al.* ( $\times$ ) with their secondary ( $p,n$ ) correction removed (no correction for oxygen contamination had been made).

### F. Uncertainties

The uncertainties associated with each of our measured cross sections can be attributed to four major sources: (1) the uncertainty in the fitted  $^{13}\text{N}$  decay curve component, (2) the error due to the subtraction of a  $^{13}\text{N}$  contribution attributed to the  $^{16}\text{O}$  contamination of the target, (3) the uncertainty in the  $^{12}\text{C}(\pi^+, \pi N)^{11}\text{C}$  cross sections and the statistical accuracy of the measurements used to determine the pion beam flux, and (4) the error introduced by the correction for the secondary ( $p,n$ ) reaction. The uncertainty in the fitted  $^{13}\text{N}$  activity contributed an average of  $\pm 0.03$  mb to the single-charge-exchange cross section. The uncertainty in the oxygen-related  $^{13}\text{N}$  contributed  $\pm 0.01$ – $0.11$  mb to the total error. This was one of the largest sources of error, considering the small percentage of oxygen present in the targets. The error in the beam flux monitor cross sections contributed an additional uncertainty of  $\pm 0.01$ – $0.11$  mb. The corrections to the secondary ( $p,n$ ) reaction were assigned an uncertainty of  $\pm 50\%$ . The combined uncertainties from all of the sources described above produced total errors of  $\pm 0.02$ – $0.15$  mb in the final cross sections.

### III. RESULTS

The cross sections for the  $^{13}\text{C}(\pi^+, \pi^0)^{13}\text{N}(\text{g.s.})$  reaction, determined in this study as described above are grouped according to incident pion energy and listed as weighted average cross sections in Table I. The measured excitation function for this reaction is shown in Fig. 4. Several features of the excitation function are worth noting. First, the cross section decreases rapidly above 50 MeV, reaching a minimum value near 70 MeV. Above 70 MeV

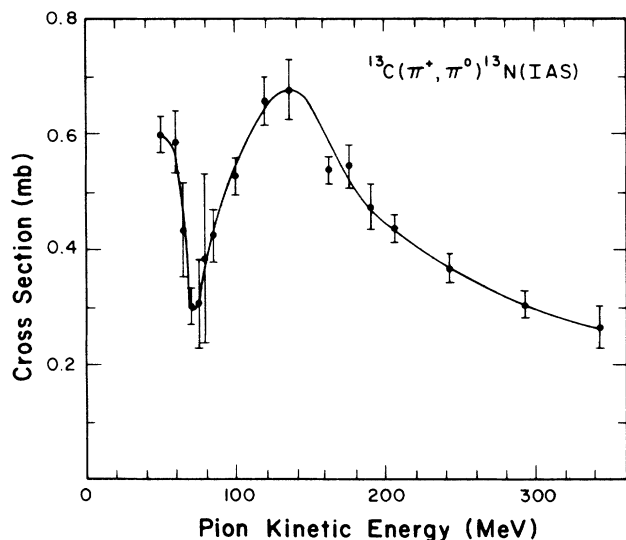


FIG. 4. Measured excitation function for the  $^{13}\text{C}(\pi^+, \pi^0)^{13}\text{N}$  (g.s.) reaction. The smooth curve is to guide the eye.

the cross section increases and reaches a maximum value at approximately 140 MeV. Beyond this energy the cross section decreases slowly and smoothly as a function of incident pion energy out to 350 MeV. Our cross-section values are found to be consistently smaller by  $\sim 0.3$  mb than those reported by Shama *et al.*<sup>4</sup> Our result of  $0.54 \pm 0.02$  mb at 164 MeV agrees with the angle-integrated cross section of  $0.72 \pm 0.18$  mb determined

from differential cross-section measurements made with the LAMPF  $\pi^0$  spectrometer.<sup>29</sup>

One possible source of the difference between our results and those of Shama *et al.*<sup>4</sup> could be a substantial oxygen contamination of their  $^{13}\text{C}$  target. In their data analysis, an attempt was made to fit a decay component of  $^{15}\text{O}$ , which is a signature for oxygen contamination, but no significant improvement to their decay curve fit was observed. In an effort to estimate the extent of oxygen contamination in a target such as that used by Shama *et al.*, we prepared several  $^{13}\text{C}$  powder targets contained in beryllium cans. These targets were irradiated with a 190-MeV  $\pi^-$  beam, and the yield of  $^{15}\text{O}$  was determined by counting them as soon as possible (2–3 min) after the irradiation. The results of these irradiations indicated that the amount of oxygen contamination in the powder targets is several percent. In our worst case, an oxygen contamination of 3% by weight was determined. The most likely source of oxygen contamination is expected to be water vapor adsorbed by the carbon powder. Because the reaction cross sections for producing  $^{13}\text{N}$  from oxygen are one order of magnitude larger than the pion single-charge-exchange cross sections of interest, this amount of oxygen contamination requires serious consideration. For example, for an incident pion energy of 164 MeV, a measured  $^{13}\text{C}(\pi^+, \pi^0)^{13}\text{N}$  cross section of 1 mb is reduced to 0.79 mb after accounting for the  $^{13}\text{N}$  contribution from an oxygen contamination of three percent by weight. Thus an oxygen contamination in the order of 5% in the target of Shama *et al.* could account for most of the discrepancy

TABLE I. Cross sections for the  $^{13}\text{C}(\pi^+, \pi^0)^{13}\text{N}$  reaction.

Pion energy <sup>a</sup> (MeV)	Number of measurements	Range of secondary ( $p, n$ ) correction (mb) <sup>b</sup>	Cross section <sup>c</sup> (mb)
50	9	0.01–0.04	$0.60 \pm 0.03$
60	4	0.03–0.06	$0.58 \pm 0.05$
65	2	0.03	$0.43 \pm 0.08$
70	6	0.02–0.07	$0.30 \pm 0.03$
75	2	0.04	$0.31 \pm 0.08$
80	2	0.03	$0.38 \pm 0.15$
85	3	0.05–0.10	$0.42 \pm 0.05$
100	6	0.04–0.08	$0.53 \pm 0.03$
119	4	0.05–0.11	$0.66 \pm 0.04$
136	4	0.05–0.12	$0.68 \pm 0.05$
162	14	0.05–0.21	$0.54 \pm 0.02$
176	5	0.05–0.12	$0.54 \pm 0.04$
190	3	0.08–0.15	$0.47 \pm 0.04$
206	8	0.05–0.16	$0.43 \pm 0.02$
243	7	0.05–0.11	$0.37 \pm 0.03$
293	8	0.03–0.11	$0.30 \pm 0.02$
343	5	0.03–0.07	$0.26 \pm 0.04$ <sup>d</sup>

<sup>a</sup>Average pion kinetic energy.

<sup>b</sup>The numbers reported in this column show the range of the secondary ( $p, n$ ) correction corresponding to the particular target thickness used (40–570 mg/cm<sup>2</sup>).

<sup>c</sup>These cross sections have been corrected for beam interruptions, oxygen contamination in each target, and for secondary ( $p, n$ ) reactions. The error bars include the uncertainties in the monitor reaction cross sections.

<sup>d</sup>This cross section also includes a correction for a  $2 \pm 2\%$  proton contamination of the beam.

between their reported cross sections and ours. Possibly at the much lower beam intensities used by Shamai *et al.* a small  $^{15}\text{O}$  component could have been missed.

In order to characterize the minimum we observed in the single-charge-exchange excitation function, we fit a simple quadratic function of the pion kinetic energy to the cross sections in the energy range from 50 to 100 MeV. The results of this parabolic fit are (1) the minimum occurs at  $75 \pm 2$  MeV, (2) the minimum cross section is  $0.34 \pm 0.12$  mb, and (3) the width of the minimum is  $33 \pm 9$  MeV. For each pion beam energy the finite momentum width of the beam leads to a spread in the energy of the pions incident on the target. This energy spread can have a relatively large effect on the measured cross section if the excitation function exhibits some degree of structure. In the present case, the effect should be most important in the region near 70 MeV where the excitation function exhibits a minimum. Here we estimated the energy spread to be a maximum of 4.7 MeV, which leads to a negligible effect of about 0.46% on the measured minimum cross section.

The location of the minimum in the  $^{13}\text{C}$  integrated cross section is about 20 MeV higher in energy than the location of the analogous minima in the zero-degree differential cross sections for light nuclei.<sup>30-32</sup> The shift in energy of this feature can be simply explained. If one looks at the location in angle of the minimum in the differential cross sections as a function of pion energy, it is seen that at 50 MeV the minimum occurs very near  $0^\circ$ , and as the energy increases, it moves out to larger angles. For the  $^{15}\text{N}(\pi^+, \pi^0)^{15}\text{O}$  reaction the minimum is at  $0^\circ$  for 48 MeV,<sup>33</sup> but at 55.5 MeV it has shifted to  $\sim 25^\circ$ . If the differential cross section is integrated over angle, a  $\sin\theta$  term comes in and gives angles near  $90^\circ$  a larger weight than angles near  $0^\circ$ . This results in shifting the minimum toward higher energies in the angle-integrated cross section, as we observed.

It is interesting to compare our angle-integrated cross section obtained at 50 MeV for the  $^{13}\text{C}(\pi^+, \pi^0)^{13}\text{N}$  SCX reaction to that measured at 48 MeV for the  $^{15}\text{N}(\pi^+, \pi^0)^{15}\text{O}$  reaction with the  $\pi^0$  spectrometer.<sup>33</sup> These latter measurements give an angle-integrated cross section of  $0.43 \pm 0.07$  mb that compares well to our values  $0.60 \pm 0.03$  mb. The similarity of these two measured cross sections can be attributed, as least in part, to the fact that both targets are  $p$ -shell nuclei with one valence nucleon involved in the charge exchange. Differences in the cross sections are probably due to detailed nuclear structure differences.

Another noteworthy feature of the  $^{13}\text{C}(\pi^+, \pi^0)^{13}\text{N}$  excitation function is that the cross section reaches a maximum value near 140 MeV after which it decreases smoothly as a function of the incident pion energy. The decreasing cross sections in the region of the (3,3) pion-nucleon resonance ( $\sim 180$  MeV) indicate that the nuclear medium has a significant effect on the SCX process.

#### IV. DISCUSSION

Of the numerous theoretical calculations that have been carried out for the  $^{13}\text{C}(\pi^+, \pi^0)^{13}\text{N}$  reaction, we have

chosen three, shown in Fig. 5, as representative of current models. These include the fixed-scatterer calculations of Kaufmann and Gibbs,<sup>5</sup> the covariant coupled-channel calculation of Liu<sup>6</sup> and the isobar-hole predictions of Hirata.<sup>7</sup> none of these calculations are found to be in good agreement with the observed excitation function, however, those of Kaufmann and Gibbs agree best with our measurements. Their calculations are done using the distorted-wave impulse approximation and include energy shifts and Pauli blocking to describe on-shell corrections and intermediate-state propagation to describe off-shell corrections. The calculation does not include spin-flip charge exchange or first-excited state contributions.

The calculation of Liu<sup>6</sup> uses a momentum space coupled-channel formalism and includes first- and second-order pion-nucleus strong interactions and the pion-nucleus Coulomb interaction. The first-order interaction is calculated using a covariant, nonstatic theory. Contributions to the second-order interaction are determined for two-nucleon processes related to true pion absorption and for scattering of pions from a correlated pair of nucleons. The curve in Fig. 5 represents the case in which the second-order potential is due solely to pion scattering from correlated nucleon pairs. This calculation emphasizes the effect of second-order contributions to the SCX cross section. However, in Ref. 6 the calculation that includes only first-order terms gives the closest reproduction of the experimental excitation function.

The calculation of Hirata<sup>7</sup> is a nonstatic theory based on the delta-hole formalism. This calculation includes recoil and binding corrections to the pion-nucleon amplitude to define the Hamiltonian of the delta and also includes the spreading potential for the delta and the Pauli-quenching effect for the decay of the delta into a pion and a nucleon. Without the spreading potential and

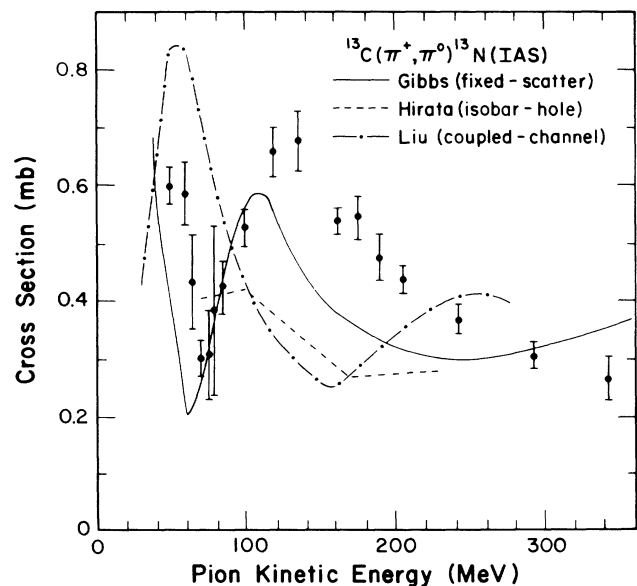


FIG. 5. Three theoretical excitation functions for the  $^{13}\text{C}(\pi^+, \pi^0)^{13}\text{N}$  reaction compared to our measured cross sections (see text).

the Pauli-quenching effect, this theory predicts an excitation function which peaks at 100 MeV and declines steadily out to 180 MeV. When the spreading potential and Pauli quenching are added the theory predicts an excitation function that peaks near 100 MeV.

All of the calculations described above underestimate the reaction cross section in the region of the (3,3) resonance by a factor of  $\sim 2$ . Because pions interact so strongly with nuclear matter in this energy range, this discrepancy probably indicates that other more complicated reaction mechanisms should be included in the calculations. The sharp dip observed at  $\sim 70$  MeV is not predicted by Liu or Hirata, but the prediction of Kaufmann and Gibbs does show a minimum at  $\sim 50$  MeV. The free  $\pi$ -nucleon charge-exchange cross section has a deep forward-angle minimum near 50 MeV that results from a nearly complete cancellation between the  $s$ - and  $p$ -wave scattering amplitudes. This phenomenon persists for SCX in nuclei, producing an analogous forward-angle minimum<sup>30</sup> and a minimum in the energy dependence of the angle-integrated cross section. The location of this minimum is influenced by nuclear medium effects that can change the relative strength of the  $s$ - and  $p$ -wave amplitudes and thus shift the energy and/or angle at which the cancellation is observed.

Figure 6 illustrates that  $s$ -wave and  $p$ -wave interference produces a minimum near 70 MeV. Shown are the results of plane-wave calculations of the angle-integrated  $^{13}\text{C}$  SCX cross section with  $s$  wave only,  $p$  wave only, and with both. The  $s$  wave, which decreases with energy, interferes destructively with the  $p$  wave, which increases with energy, to produce a minimum near 70 MeV. The plane-wave calculations were done with Siciliano's program DWPIES (Ref. 34) with the distortions turned off and with the "FP85" phase-shift solution of Arndt.<sup>35</sup> We expect that if distortions were added to this calculation it

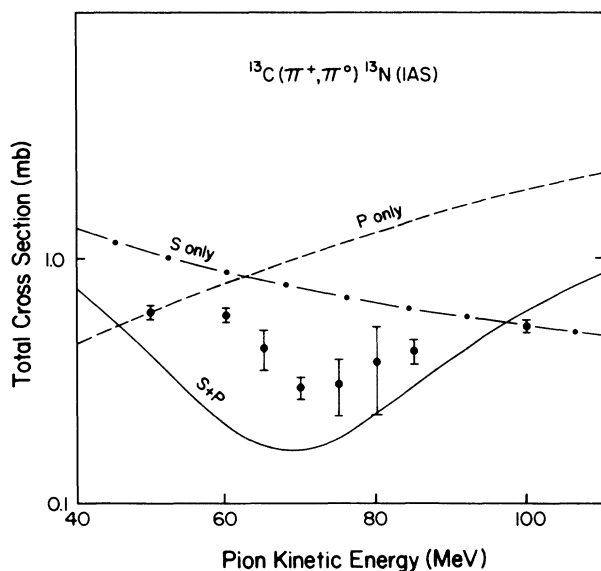


FIG. 6. Plots of results of plane-wave calculations of the angle-integrated  $^{13}\text{C}$  SCX cross section with  $s$  wave only,  $p$  wave only, and with both. The data points are from this study.

would tend to wash out the minimum and cause it to be less deep.

We believe that further theoretical efforts in interpreting these measurements will contribute to an improved understanding of pion-induced single-charge-exchange reactions.

#### ACKNOWLEDGMENTS

We express our gratitude to Dr. D. C. Hagerman and the accelerator-operations team at LAMPF for their cooperation and support. We also thank Dr. D. C. Hoffman, Dr. J. E. Sattizahn, Dr. D. W. Barr, and Dr. W. R. Daniels for their encouragement and support. One of us (N.I.) would like to thank Group INC-11 and Dr. L. Rosen and his staff for their kind hospitality during his stay at Los Alamos. This work has been performed under the auspices of the Division of Nuclear Physics of the U.S. Department of Energy.

#### APPENDIX

In an effort to estimate the contribution to the  $^{13}\text{N}$  yield from secondary ( $p, n$ ) reactions, we developed an extensive analytical formalism that enabled computer calculations of the  $^{13}\text{C}(p, n)^{13}\text{N}$  yield to be made. The formalism is a more precise and refined approach to the method used by Koch.<sup>36</sup> The probability for a secondary ( $p, n$ ) reaction to occur depends on the production of secondary protons and on the ( $p, n$ ) cross section. The total secondary reaction contribution is obtained by integrating over the dimensions of the target and over the secondary proton energy and angular distribution. The approach is outlined below.

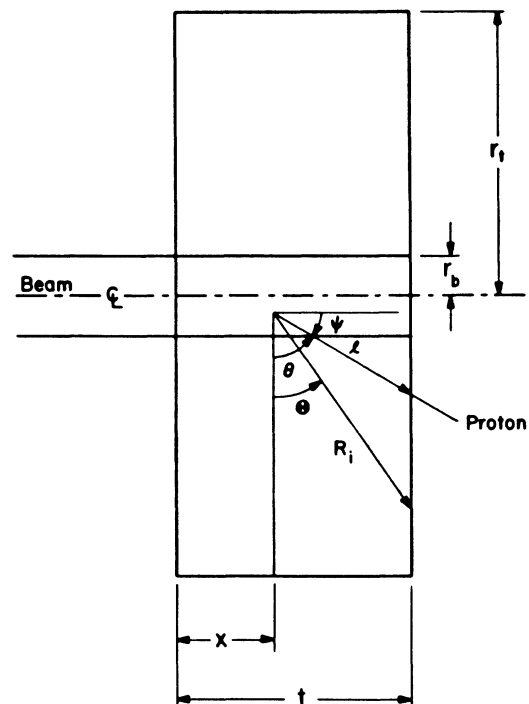


FIG. 7. Side view of beam and target to define the parameters used in the derivation of Eq. (A2).

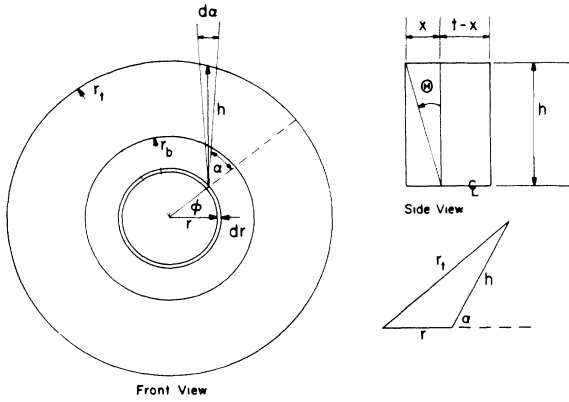


FIG. 8. Front view of beam and target to define the parameters used in the derivation of Eq. (A4). Side view shows volume of target with which a selected secondary proton can interact.

The probability for a  $(p,n)$  reaction to occur over a proton path length  $l$  inside the target is given by the expression

$$P(l) = 1 - \exp \left[ - \int_0^l n \sigma_{p,n}(u) du \right]. \quad (\text{A1})$$

Here,  $n$  is the number of target nuclei per unit volume, and  $\sigma_{p,n}(u)$  is the cross section for the  $(p,n)$  reaction as a function of distance traveled inside the target, where  $\sigma(E_p^{\text{init}}) = \sigma(u=0)$ . The range-energy curves of Ref. 28 were used to convert energies to ranges for protons in the target material.

It was assumed that the proton angular distribution was cylindrically symmetric and forward peaked with the form

$$f(\psi) = a_0 + a_1 \cos \psi.$$

However, when integrated over target thickness  $t$  and angles  $\psi = 0^\circ$  to  $180^\circ$ , the anisotropies in the angular distribution are averaged out, giving the same results as an isotropic angular distribution, which was used in the calculation.

Only protons with energies greater than the threshold energy (3.24 MeV for  $^{13}\text{C}$ ) for the  $(p,n)$  reaction need to

$$\langle P(t, E_p) \rangle = \begin{cases} \frac{1}{t} \int_0^t G(x) dx + \frac{t}{2R_i} \left[ 1 - \exp \left[ - \int_0^{R_i} n \sigma_{p,n}(u) du \right] \right] & \text{for } t \leq R_i, \\ \frac{1}{t} \int_0^{R_i} G(x) dx + \left[ 1 - \frac{R_i}{2t} \right] \left[ 1 - \exp \left[ - \int_0^{R_i} n \sigma_{p,n}(u) du \right] \right] & \text{for } t > R_i. \end{cases} \quad (\text{A2})$$

The first term in Eq. (A2) results from protons that escape from the target with energy exceeding the threshold energy and the second term comes from the protons that range out in the target. Finally, by combining Eq. (A2) with the secondary proton production cross section,  $\sigma_{\pi,p}(E_p)$  for the reaction  $\pi^+ + ^{13}\text{C} \rightarrow p + X$ , and integrating over the secondary proton energy distribution, the secondary cross section as a function of target thickness is given as

$$\sigma_{\text{sec}}(t) = \int_{E_p^{\text{thresh}}}^{E_p^{\text{max}}} \sigma_{\pi,p}(E_p) \langle P(t, E_p) \rangle dE_p. \quad (\text{A3})$$

In our calculation, the  $(p,n)$  excitation function data were taken from Refs. 24–26 and the secondary proton yields were calculated by means of the ISOBAR (Ref. 21) intranuclear cascade code and DFF (Ref. 22) evaporation code.

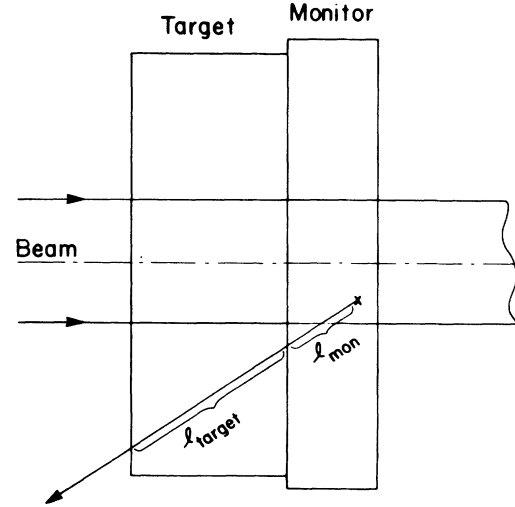


FIG. 9. Schematic diagram of target and monitor configuration.

be included in the calculation. For this reason, an interaction range  $R_i$  is introduced that subtracts out the threshold range of the protons, i.e.,  $R_i = R(E_p) - R(E_p^{\text{thresh}})$ . Range-straggling effects have been ignored, and straight-line trajectories for the proton paths were assumed. Figure 7 is included to facilitate the discussion of the distance and angular parameters over which the integration is performed.

Generalizing Eq. (A1) to include the angular integration, we define

$$G(x) \equiv \int_{\Theta}^{\pi/2} F(x, \theta) \cos \theta d\theta, \\ F(x, \theta) \equiv 1 - \exp \left[ - \int_0^{(t-x)/\sin \theta} n \sigma_{p,n}(u) du \right],$$

where  $l = (t-x)/\sin \theta$  and  $\Theta = \sin^{-1}(t-x)/R_i$ . For the case where the interaction range  $R_i$  is less than or equal to the difference between the target radius  $r_t$  and the beam radius  $r_b$  (i.e.,  $R_i \leq r_t - r_b$ , the infinite target radius case), we can write the  $(p,n)$  reaction probability for protons of energy  $E_p$  and for a target thickness  $t$  as

The formalism was subsequently generalized to consider the effect of the finite beam radius on the secondary reaction contribution (i.e., to include cases where  $R_i > r_t - r_b$ ). Figure 8 defines the geometry of the problem. To calculate the average  $(p, n)$  reaction probability as a function of proton energy  $E_p$  and target thickness  $t$  for a target of radius  $r_t$ , we integrated the secondary reaction probability function  $P(t, E_p)$  given in Eq. (A3) over angle  $\alpha$  and radius  $r$ .

The average probability for a  $(p, n)$  secondary reaction to occur inside the target as a result of a proton originating anywhere inside the beam volume within the target (a uniform beam distribution with beam radius  $r_b$  is assumed) is then computed as follows:

$$\langle P'(t, E_p) \rangle = 2 \cdot \int_{r_{\min}}^{r_b} \frac{2\pi r dr}{\pi r_b^2} \cdot \left[ \frac{(\pi - \alpha_{\max})}{2\pi} \langle P(t, E_p) \rangle + \int_0^{\alpha_{\max}} \langle P(t, E_p, r, \alpha) \rangle \frac{d\alpha}{2\pi} \right] + \frac{r_{\min}^2}{r_b^2} \langle P(t, E_p) \rangle, \quad (\text{A4})$$

where the integration limits  $r_{\min}$  and  $\alpha_{\max}$  are defined as

$$r_{\min} \equiv r_t - R_i, \\ \alpha_{\max} \equiv \cos^{-1}(r_t^2 - r^2 - R_i^2)/2rR_i.$$

For high-energy protons,  $r_{\min}$  becomes equal to zero and  $\alpha_{\max} = \pi$ . The factor of 2 preceding the integral in (A4) is explained by the fact that the same length  $h$  occurs twice, once for each sign of the angle  $\alpha$ .

Another component to the secondary  $(p, n)$  correction comes from the secondary protons originating in the pion beam monitor disk located just downstream of the  $^{13}\text{C}$  target. Consider a proton originating in the monitor as shown in Fig. 9. The distance  $l_{\text{mon}}$  traveled by this proton inside the monitor is first reduced to an equivalent target distance  $l_{\text{mon}}^*$  according to the ratio of monitor-to-target densities,

$$l_{\text{mon}}^* = \frac{n_{\text{mon}}}{n_{\text{targ}}} \cdot l_{\text{mon}}.$$

For this experiment, the density ratio is 0.7765.

If we then define  $l_{\text{tot}} \equiv l_{\text{targ}} + l_{\text{mon}}^*$ , the probability for a  $(p, n)$  reaction to occur within the target as a result of secondary protons originating in the monitor is given by

$$\langle P''(t, E_p) \rangle = \left[ 1 - \exp \left[ - \int_0^{l_{\text{tot}}} n \sigma_{p,n}(u) du \right] \right] - \left[ 1 - \exp \left[ - \int_0^{l_{\text{mon}}^*} n \sigma_{p,n}(u) du \right] \right]. \quad (\text{A5})$$

Because the ISOBAR-DFP calculations indicated that the cascade protons are forward peaked, only evaporation protons originating in the monitor and emitted in the backward hemisphere were included in these calculations.

The total average probability for secondary  $(p, n)$  reactions to occur within the target as a result of protons originating anywhere inside the beam cylinder intercepted by the target and monitor can be defined as the sum of the contributions calculated with Eqs. (A2), (A4), and (A5), i.e.,

$$\langle P_{\text{tot}}(t, E_p) \rangle = \begin{cases} \langle P(t, E_p) \rangle + \langle P''(t, E_p) \rangle & \text{for } R_i \leq r_t - r_b, \\ \langle P'(t, E_p) \rangle + \langle P''(t, E_p) \rangle & \text{for } R_i > r_t - r_b. \end{cases} \quad (\text{A6})$$

Thus the secondary  $(p, n)$  reaction cross section as a function of target thickness is given by

$$\sigma_{\text{sec}}(t) = \int_{E_p^{\text{thresh}}}^{E_p^{\text{max}}} \sigma_{\pi,p}(E_p) \langle P_{\text{tot}}(t, E_p) \rangle dE_p, \quad (\text{A7})$$

where  $\sigma_{\pi,p}(E_p)$  is the cross section for proton production by the pion beam as calculated with the ISOBAR/DFP codes.

The choice for  $E_p^{\text{max}}$  depended on the pion kinetic energies, in the sense that further increases in  $E_p^{\text{max}}$  changed  $\sigma_{\text{sec}}(t)$  insignificantly. The results of these secondary reaction cross-section calculations for the  $^{13}\text{C}(p, n)^{13}\text{N}$  reaction are shown in Table I and Figs. 2 and 3. For further details of these calculations, see Ref. 19.

\*Present address: Group N-2, Los Alamos National Laboratory, Los Alamos, NM 87545.

†Present address: Group X-2, Los Alamos National Laboratory, Los Alamos, NM 87545.

‡Present address: Kyoto University, Sakyo-Ku, Kyoto 606, Japan.

§Present address: Group P-2, Los Alamos National Laboratory, Los Alamos, NM 87545.

‖J. Alster and J. Warszawski, Phys. Rep. **52**, 87 (1979).

<sup>2</sup>Los Alamos Scientific Laboratory Report No. LA-7892-C, 1979.

<sup>3</sup>D. T. Chivers, E. M. Rimmer, B. W. Allerdycce, R. C. Witcomb, J. J. Domingo, and N. W. Tanner, Nucl. Phys. **A126**, 129 (1969).

<sup>4</sup>Y. Shamaï, J. Alster, D. Ashery, S. Cochavi, M. A. Moinester, A. I. Yavin, E. D. Arthur, and D. M. Drake, Phys. Rev. Lett. **36**, 82 (1976).

<sup>5</sup>W. B. Kaufmann and W. R. Gibbs, Phys. Rev. C **28**, 1286

- (1983).
- <sup>6</sup>L. C. Liu, *Phys. Rev. C* **23**, 814 (1981).
- <sup>7</sup>M. Hirata, *Phys. Rev. C* **24**, 1604 (1981).
- <sup>8</sup>R. E. Anderson, J. J. Krauschaar, E. Rost, and D. A. Sparrow, University of Colorado Annual Report, 1976.
- <sup>9</sup>R. L. Burman, R. Fulton, and M. Jacobson, *Nucl. Instrum. Methods* **131**, 29 (1975).
- <sup>10</sup>R. D. Werbeck and R. J. Macek, *IEEE Trans. Nucl. Sci.* **22**, 1958 (1975).
- <sup>11</sup>B. J. Dropesky, G. W. Butler, C. J. Orth, R. A. Williams, M. A. Yates-Williams, G. Friedlander, and S. B. Kaufman, *Phys. Rev. C* **20**, 1844 (1979).
- <sup>12</sup>Los Alamos National Laboratory Document No. MP-DO-3-UHB (Rev.), 1984.
- <sup>13</sup>M. Zaider, J. Alster, D. Ashery, N. Auerbach, S. Cochavi, M. A. Moinester, J. Warszawski, and A. I. Yavin, in *Proceedings of the 5th International Conference on High Energy Physics and Nuclear Structure, Uppsala, Sweden, 1973*, edited by G. Tibell (American Elsevier, New York, 1973), pp. 219–222.
- <sup>14</sup>Formerly produced by Pilot Chemicals Division, New England Nuclear Corp., Watertown, MA, but currently manufactured by Bicron Corp., Newbury, OH.
- <sup>15</sup>G. W. Butler, B. J. Dropesky, C. J. Orth, R. E. L. Green, R. G. Korteling, and G. K. Y. Lam, *Phys. Rev. C* **26**, 1737 (1982).
- <sup>16</sup>L. P. Remsberg, *Ann. Rev. Nucl. Sci.* **17**, 347 (1963).
- <sup>17</sup>N. P. Jacob and S. S. Markowitz, *Phys. Rev. C* **13**, 754 (1976).
- <sup>18</sup>J. B. Cumming, USAEC Report No. NAS-NS-3017, 1963.
- <sup>19</sup>J. J. H. Berlijn (unpublished).
- <sup>20</sup>These calculations were performed by L. C. Liu, private communication, Los Alamos National Laboratory.
- <sup>21</sup>G. D. Harp, K. Chen, G. Friedlander, Z. Fraenkel, and J. M. Miller, *Phys. Rev. C* **8**, 581 (1973); J. N. Ginocchio, *ibid.* **17**, 195 (1978).
- <sup>22</sup>I. Dostrovsky, Z. Fraenkel, and G. Friedlander, *Phys. Rev. C* **116**, 683 (1959).
- <sup>23</sup>A. S. Carroll, I. H. Chiang, C. B. Dover, T. F. Kycia, K. K. Li, P. O. Mazur, D. N. Michael, P. M. Mockett, D. C. Rahm, and R. Rubenstein, *Phys. Rev. C* **14**, 635 (1976).
- <sup>24</sup>D. A. Lind, R. J. Peterson, and H. W. Fielding, *Phys. Rev. C* **11**, 2099 (1975).
- <sup>25</sup>P. Dagley, W. Haeberli, and J. X. Saladin, *Nucl. Phys.* **24**, 353 (1961).
- <sup>26</sup>L. Valentin, *Nucl. Phys.* **62**, 81 (1965).
- <sup>27</sup>T. E. Ward, C. C. Foster, and G. E. Walker, *Phys. Rev. C* **25**, 762 (1982).
- <sup>28</sup>C. F. Williamson, J. P. Boujot, J. Picard, Centre d'etudes nucléaires de Saclay Rapport CEA-R3042, 1966.
- <sup>29</sup>A. Doran, J. Alster, A. Errell, M. A. Moinester, R. A. Anderson, H. W. Baer, J. D. Bowman, M. D. Cooper, F. H. Cverna, C. M. Hoffman, N. S. P. King, M. J. Leitch, J. Piffaretti, and C. D. Goodman, *Phys. Rev. C* **26**, 189 (1982).
- <sup>30</sup>F. Irom, H. W. Baer, J. D. Bowman, M. D. Cooper, U. Sennhauser, H. J. Ziocck, M. J. Leitch, A. Errell, M. A. Moinester, and J. R. Comfort, *Phys. Rev. C* **31**, 1464 (1985).
- <sup>31</sup>J. L. Ullman, P. W. F. Alons, J. J. Kraushaar, J. H. Mitchell, R. J. Peterson, R. A. Ristinen, J. N. Knudson, J. R. Comfort, H. W. Baer, J. D. Bowman, M. D. Cooper, D. H. Fitzgerald, F. Irom, M. J. Leitch, and E. Piasetzky, *Phys. Rev. C* **33**, 2092 (1986).
- <sup>32</sup>F. Irom, M. J. Leitch, H. W. Baer, J. D. Bowman, M. D. Cooper, B. J. Dropesky, E. Piasetzky, and J. N. Knudson, *Phys. Rev. Lett.* **55**, 1862 (1985).
- <sup>33</sup>M. D. Cooper, H. W. Baer, R. Bolton, J. D. Bowman, F. Cverna, N. S. P. King, M. Leitch, J. Alster, A. Doron, A. Errell, M. A. Moinester, E. Blackmore, and E. R. Siciliano, *Phys. Rev. Lett.* **52**, 1100 (1984).
- <sup>34</sup>E. R. Siciliano, M. D. Cooper, M. B. Johnson, and M. J. Leitch, *Phys. Rev. C* **34**, 267 (1986).
- <sup>35</sup>Program SAID (Scattering Analysis Interactive Dialin), R. A. Arndt, Virginia Polytechnic Institute and State University, 1985.
- <sup>36</sup>R. C. Koch, Ph.D. thesis, University of Chicago, 1955.